Supplemental Materials

Surface Interactions with Compartmentalized Cellular Phosphates Explain Rare Earth Oxide Nanoparticle Hazard and Provide Opportunities for Safer Design

Ruibin Li[†], Zhaoxia Ji[‡], Chong Hyun Chang[‡], Darren R. Dunphy[§], Xiaoming Cai[⊥], Huan Meng[†], Haiyuan Zhang[‡], Bingbing Sun[†], Xiang Wang[‡], Juyao Dong[∥], Sijie Lin[‡], Meiying Wang[†], Yu-Pei Liao[†], C. Jeffrey Brinker[§], Andre Nel[†,‡,*], and Tian Xia[†,‡,*]

[†]Division of NanoMedicine, Department of Medicine, University of California, 10833 Le Conte Avenue, Los Angeles, California 90095, United States, [‡]California NanoSystems Institute, University of California, 570 Westwood Plaza, Los Angeles, California 90095, United States, [§]Department of Chemical and Nuclear Engineering, Engineering, University of New Mexico, University of New Mexico MSC01 1120, Albuquerque, New Mexico 87131, United States, [⊥]Department of Pharmacology, School of Medicine, University of California, 360 Med Surge II, Irvine, California 92697, [∥]Department of chemistry & Biochemisty, University of California, 607 Charles E. Young Drive East, Los Angeles, California 90095, United States.

*Corresponding Author: Tian Xia, Ph.D.; and Andre Nel, Ph.D.

Department of Medicine, Division of NanoMedicine, UCLA School of Medicine, 52-175 CHS, 10833 Le Conte Ave, Los Angeles, CA 90095-1680.
Tel: (310) 983-3359, Fax: (310) 206-8107
E-mail: txia@ucla.edu
Anel@mednet.ucla.edu

Table S1. Primary and Hydrodynamic Nanoparticle Sizes

Nanoparticles	Primary Size (nm)	Hydrodynamic Size in Media (nm)		
		Water	c-RPMI 1640	PBS + BSA
Al_2O_3	14.7 ± 5.2*	492.3 ± 103.4	313.6 ± 67.3	469.4 ± 34.7
Bi_2O_3	27.4 ± 8.7	676.5 ± 112.5	590.1 ± 57.3	688.7 ± 26.6
CeO_2	18.3 ± 6.8*	413.5 ± 196.6	306.8 ± 82.3	427.0 ± 50.3
CoO	71.8 ± 16.2*	1247.9 ± 244.8	477.6 ± 76.6	1028.4 ± 42.4
Co_3O_4	10.0 ± 2.4*	166.0 ± 19.4	261.9 ± 6.7	334.4 ± 53.6
Cr_2O_3	193.0 ± 90.0*	873.1 ± 343.8	695.6 ± 165.4	534.9 ± 44.9
CuO	12.8 ± 3.4*	575.7 ± 265.4	571.4 ± 96.0	505.4 ± 74.4
Dy_2O_3	37.5 ± 6.6	898.5 ± 452.6	707.5 ± 170.5	705.3 ± 101.6
Er_2O_3	113.8 ± 37.8	385.4 ± 52.7	362.6 ± 21.5	415.3 ± 27.8
Eu_2O_3	52.8 ± 11.7	601.9 ± 239.5	504.8 ± 53.0	568.2 ± 32.5
Fe_2O_3	12.3 ± 2.9*	255.3 ± 14.2	304.6 ± 27.8	282.7 ± 7.8
Fe_3O_4	12.0 ± 3.2*	346.2 ± 31.0	415.7 ± 97.7	328.3 ± 75.3
Gd_2O_3	43.8 ± 15.8*	820.1 ± 277.5	408.5 ± 17.9	814.1 ± 68.3
HfO_2	28.4 ± 7.3*	365.6 ± 20.3	341.3 ± 9.4	303.5 ± 8.7
In_2O_3	59.6 ± 19.0*	236.3 ± 7.7	225.8 ± 20.2	231.0 ± 29.5
La_2O_3	24.6 ± 5.3*	806.6 ± 339.2	378.2 ± 33.1	821.8 ± 43.0
Nd_2O_3	133.8 ± 51.6	829.0 ± 78.7	573.3 ± 93.8	660.6 ± 46.8
NiO	13.1 ± 5.9*	633.1 ± 116.7	345.1 ± 16.4	366.5 ± 62.4
Ni_2O_3	140.2 ± 52.5*	664.4 ± 144.4	468.6 ± 104.9	914.4 ± 255.5
Sb_2O_3	11.8 ± 3.8*	222.7 ± 8.4	260.8 ± 20.7	253.2 ± 94.3
Sm_2O_3	108.3 ± 47.4	770.7. ± 96.3	682.4 ± 78.4	762.4 ± 59.6
SnO_2	64.2 ± 13.2*	445.8 ± 161.8	490.8 ± 178.9	473.3 ± 148.0
TiO_2-Anatase	12.6 ± 4.3*	203.5 ± 15.7	307.6 ± 39.3	374.6 ± 122.9
WO_3	16.6 ± 4.3*	104.6 ± 4.6	133.0 ± 6.1	118.2 ± 44.2
Y_2O_3	32.7 ± 8.1*	1345.7 ± 194.9	451.0 ± 117.1	659.1 ± 139.0
Yb_2O_3	61.7 ± 11.3*	513.3 ± 382.6	330.9 ± 70.9	659.7 ± 227.3
ZnO	22.6 ± 5.1*	210.3 ± 2.3	320.1 ± 4.9	453.4 ± 13.6
ZrO_2	40.1 ± 12.6*	494.4 ± 97.6	214.3 ± 18.9	224.0 ± 27.4

* Zhang *et al.* ACS Nano 2012, 6, 4369-4368.

Table S2. Sources and Isoelectric Points of Nanoparticles

Nanoparticles	Vendor	IEP	ζ at pH 7.4 (mV)
Al_2O_3	Meliorum	7.4	0
Bi_2O_3	Lutz Madler*	2.0	−22.7
CeO_2	Meliorum	7.8	21.4
CoO	US-Nano	9.2	21.6
Co_3O_4	Lutz Madler	9.4	24.6
Cr_2O_3	US Nano	5.3	−32.6
CuO	Lutz Madler	7.9	7.6
Dy_2O_3	US-Nano	6.8	-16.0
Er_2O_3	US-Nano	7.4	-1.7
Eu_2O_3	US-Nano	7.7	4.5
Fe_2O_3	US Nano	7.2	−2.1
Fe_3O_4	Lutz Madler	5.0	−31.0
Gd_2O_3	NanoAmor	8.0	6.5
HfO_2	US-Nano	8.1	33.5
In_2O_3	US-Nano	9.2	61.9
La_2O_3	NanoAmor	9.4	54.3
Nd_2O_3	NanoAmor	6.4	-18.3
NiO	Sigma	11.4	27.6
Ni_2O_3	US-Nano	8.3	32.2
Sb_2O_3	Lutz Madler	1.0	−35.3
Sm_2O_3	US-Nano	7.0	-5.7
SnO_2	US Nano	4.0	−38.8
TiO_2-Anatase	Lutz Madler	6.4	−30.4
WO_3	Lutz Madler	0.3	−61.3
Y_2O_3	Meliorum	9.6	42.7
Yb_2O_3	MK-Nano	8.2	9.9
ZnO	Lutz Madler	9.6	28.8
ZrO_2	US-Nano	5.8	−12.8

*****IWT Foundation Institute of Materials Science, Department of Production Engineering, University of Bremen, Bremen, Germany.

Methods

S-1 Preparation of fluorophore loaded liposomes

Propidium iodide (PI) encapsulating liposomes were synthesized according to film rehydration method using a mini-extruder equipped with PC membrane of 100 nm pore (Avanti Polar Lipids, Alabama)[1]. Briefly, 10 mg of phosphatidic acid (Avanti, Alabaster, Alabama, USA) was dissolved in 5 mL $CHCl_3$ in a 50 mL round flask. Lipid films were made by evaporation for ~30 min, using a rotary evaporator connected to a vacuum system at room temperature. The resulting thin lipid film was placed in a chemical hood overnight to remove trace amounts of organic solvents. Subsequently, 5 mL of MOPS buffer (10 mM 3-(N-morpholino) propanesulfonic acid, 60 mM NaCl, pH 7.0) at PI concentration of 50 μg/mL was added to the flask and incubated at 37 ℃ for 2 h. In order to make homogeneous unilamellar liposomes, the multi-lamellar liposomes were repeatedly extruded at a 100 nm pore size, 11 times. In order to remove the non-trapped PI, the solution was centrifuged at 100, 000 rpm for 30 min to collect the pellet, which was resuspended in 10 mL saline buffer to yield a PI loaded liposome suspension. The liposome was characterized for size, size distribution, and zeta potential before use.

S-2 LC-MS analysis of phospholipids

Liquid chromatography (LC)-MS analysis was performed with a Surveyer LC system coupled to a LTQ-FTMS that includes electrospray ionization source (ESI) (Thermo Fisher Scientific, Waltham, MA). The MS was operated in ESI+ ionization mode with data collection from m/z 100 to 1200. For LC separation, a Luna C5 column (2.1×50 mm, 100 Å, 5 μm, Phenomenex, Los Angeles, CA) was employed with column and auto-sampler temperatures maintained at 25 ℃ and 4 ℃, respectively. Injection volumes were 3 μl. The column was eluted with a gradient of mobile phase A (methanol:50 mM ammonium formate 5:95) and mobile phase B (isopropanol:methanol:50 mM ammonium formate 60:35:5) as follows: 100% A for 5 min at 0.1 ml/min; 0-100% B over 15 min at 0.4 ml/min; 100% B for 5 min at 0.5 ml/min; 0-100% A for 5 min at 0.4 ml/min. 0.1% formic acid was added to improve the ionization.

External calibration of the FTMS was carried out with a standard LTQ calibration mixture (Thermo Scientific, Waltham, MA). The following settings were used for the FTMS: vaporizer temperature, 280 ℃; sheath and auxiliary gases, 35 and 15 (arbitrary units); spray voltage, 3.5

kV; capillary temperature, 350 ℃; capillary voltage, 10 V; tube-lens voltage, 120 V; maximum injection time, 1000 ms; maximum number of ions collected for each scan, 5×10^5; mass resolution of 100,000. MS data were recorded in centroid mode. Accurate masses of phospholipids were extracted with a mass tolerance of 10 ppm in the total ion chromatogram (TIC).

S-3 Lung inflammation and fibrosis in mice

Eight-week-old male C57Bl/6 mice purchased from Charles River Laboratories (Hollister, CA) were used for animal experiments. All animals were housed under standard laboratory conditions that have been set up according to UCLA guidelines for care and treatment of laboratory animals as well as the NIH Guide for the Care and Use of Laboratory Animals in Research (DHEW78-23). These conditions were approved by the Chancellor's Animal Research Committee at UCLA and include standard operating procedures for animal housing (filter-topped cages; room temperature at 23 ± 2 ℃; 60% relative humidity; 12 h light, 12 h dark cycle) and hygiene status (autoclaved food and acidified water). Animals were exposed by oropharyngeal aspiration as described by us[2]. Briefly, animals were anesthetized by intraperitoneal injection of ketamine (100 mg/kg)/xylazine (10 mg/kg) in a total volume of 100 μL. The anesthetized animals were held in a vertical position. 50 μL aliquots of the nanoparticle suspensions in PBS were instilled at the back of the tongue to allow pulmonary aspiration of a dose of 2 mg/kg. Each experiment included control animals, which received the same volume of PBS. The positive control in each experiment received 5 mg/kg MUS. Each group included six mice. The mice were sacrificed after 21 days. BALF and lung tissue were collected as previously described. The BALF was used for performance of total and differential cell counts and measurement of IL-1β, TGF-β1 and PDGF-AA levels. Lung tissue was stained with hematoxylin/eosin or with Masson’s Trichrome stain, and was homogenized with a Tissuemiser homogenizer (Fisher Scientific) for the assessment of the total collagen content in each lung (Sircol Collagen Assay, UK).

Figure legends

Figure S1. Morphological changes and dissolution of REO nanoparticles in PSF and acidic solutions.

A) Morphological changes of the nanoparticles after exposure to PSF. The particles were suspended in H_2O or PSF at 50 μg/mL and incubated at 37 ºC for 24 h. After washing with DI H_2O, particle morphology was observed by TEM. B) Morphology of pure La_2O_3 and as-received La_2O_3 in PSF or acidic phosphate solution at 50 μg/mL. Pure La_2O_3 was prepared by calcining the as-received La_2O_3 at 825 ℃. Both pure and as-received La_2O_3 were dispersed in PSF or 50 mM phosphate solution (pH 4.5) at 37 ℃ for 24 h. Morphological changes were observed by TEM. C) Dissolution amounts of REOs in water and acidic solution (HCl, pH 4.5). Nanoparticles were dispersed in water or HCl solution at 50 μg/mL, and incubated for 24 h at 37 ºC. After centrifugation at 15,000 rpm for 10 min, the supernatant was collected to determine the dissolved metal content using ICP-OES.

Figure S2. Subcellular localization and bio-transformation of REOs in THP-1 lysosomes.

A) Subcellular nanoparticle distribution in THP-1 cells as visualized by confocal microscopy. After cellular incubation with 12.5 μg/mL FITC-labeled nanoparticles for 12 h, the cells were washed with PBS and fixed in 4% paraformaldehyde. The nuclei were stained with Hoechst 33342 dye and the lysosomes were visualized using Alexa fluor 594-conjugated LAMP1 antibody. B) REO nanoparticle biotransformation in THP-1 cells as observed by TEM. THP-1 cells were treated with REOs at 50 μg/mL for 24 h, followed by washing, fixing and staining to prepare the TEM grids as described previously[3].

Figure S3. Establishment of a nanoparticle library that includes 10 REOs and 18 non-REO metal oxides, and comparison of their inflammatory potential

A) TEM images of the 28 nanoparticles used in this study. The particles were suspended in water at 50 μg/mL, and a drop of each particle suspension was placed on TEM grids. After drying at room temperature, the grids were observed under TEM. B) Particle endotoxin levels as determined by a standard Lonza LAL assay. All the materials exhibited endotoxin levels that are below the FDA standard for sterile water. C) Cell viability determined by MTS assay on THP-1 cells exposed to 0-50 μg/mL metal oxide particles for 24 h. D) IL-1β dose response following particle exposure for 24 h, as described

in Fig. 2B. E) Cellular uptake in THP-1 cells w/ or w/o cytochalasin D treatment. After pre-treatment by 5 μg/mL cytochalasin D for 3 h, THP-1 cells were exposed to 12.5 μg/mL FITC-labeled nanoparticles for 12 h. After thorough washing, cells were analyzed by confocal microscopy or flow cytometry to determine the abundance of cellular uptake. F) IL-1β release from THP-1 cells in the presence of cytochalasin D. IL-1β was measured in THP-1 cells pretreated with 5 μg/mL cytochalasin D for 3 h and then incubated with 50 μg/mL nanoparticles for an additional 6 h. G) IL-1β release from THP-1 cells in the presence of the cathepsin B inhibitor, CA-074-Me. After pre-treatment by 50 μM CA-074-Me for 3 h, THP-1 cells were incubated with 50 μg/mL REOs for an additional 6 h. H) IL-1β release by selected nanoparticles in wild type, NLRP3 or ASC knockout THP-1 cells. Cells were exposed to 50 μg/mL nanoparticles for 6 h. IL-1β was detected by ELISA assay. * $p < 0.05$ compared to untreated wild THP-1 cells, # $p < 0.05$ compared to wild type THP-1 cells treated with nanoparticles

Figure S4. Assessment of PDGF-AA production in a cellular co-culture system

Co-culture of THP-1 and BEAS-2B cells to detect PDGF-AA production in Corning HTS Transwell-96 plates (Corning, NY, USA), in which the upper and lower chambers are separated by a filter with 1.0 μm pore size[2]. Briefly, THP-1 (1×10^4) and BEAS-2B cells (1×10^4) were seeded in the upper and lower chamber of the transwell system, respectively. After overnight incubation, both chambers received 50 μg/mL of the indicated nanoparticle suspensions were then combined for 24 h. The supernatants were collected and used to measure PDGF-AA by a PDGF-AA Quantikine ELISA kit (R&D, MN, USA). The antibody in this can detect both the specific human and mouse growth factors. * $p < 0.05$ compared to Ctrl.

Figure S5. Schematic to illustrate the possible mechanisms of membrane damage by REOs

One possible mechanism could be the effect of nanopaticle shape, namely that the needle-like crystals on the transformed nanoparticles surface could pierce the lysosomal membrane. The second possibility is dephosphorylation of the phospholipids in the lipid bilayer, leading to disruption of the liposomal membrane.

Figure S6. IL-1β production as well as cellular uptake in THP-1 cells incubated with non-treated or PSF-treated nanoparticles

A) Cellular uptake of nanoparticles determined by ICP-OES. After 12 h treatment with 50 μg/mL nanoparticles, THP-1 cells were washed three times and lysed. The protein concentration in the lysate supernatants was determined by Bradford method and the metal elements in lysis solutions were measured by ICP-OES.[4] B) IL-1β production in THP-1 cells treated with 50 μg/mL nanoparticles for 24 h. PSF-treated nanoparticles were prepared by incubating nanoparticles in PSF for 24 h.

Figure S7. Hemolysis dose-response in RBCs induced by nanoparticles

A hemolysis assay was performed in RBCs treated with 50, 100, 200 and 400 μg/mL nanoparticles in saline w/ or w/o phosphate, as described in Fig. 3B.

Figure S8. Sub-chronic effects of the REO nanoparticles in the mouse lung.

A) Differential cell counts in bronchoalveolar lavage fluid (BALF) 21 days after the animal exposure to a one-time instillation of 2 mg/Kg of the nanoparticles. B) H&E staining of lung tissues. * $p < 0.05$ compared to Ctrl.

Figure S9. Cellular uptake of uncoated and phosphate-coated REO nanoparticles

Phosphate-coated REO particles were prepared as described in Fig. 5. THP-1 cells were incubated with 50 μg/mL REO nanoparticles w/ or w/o phosphate coating for 12 h. Then the metal elements were determined in cell lysis by ICP-OES.

Figure S10. Cytokine production in BALF and total collagen in lungs exposed to phosphate-coated REOs after 21 days

A) Assessment of IL-1β, TGF-β1 and PDGF-AA levels in the BALF 21 days after exposure to 2 mg/kg La_2O_3, Gd_2O_3, phosphate-coated La_2O_3 or phosphate-coated Gd_2O_3. B) Trichrome staining of the lung tissue. * $p < 0.05$ compared to uncoated REOs.

Figure S1

A

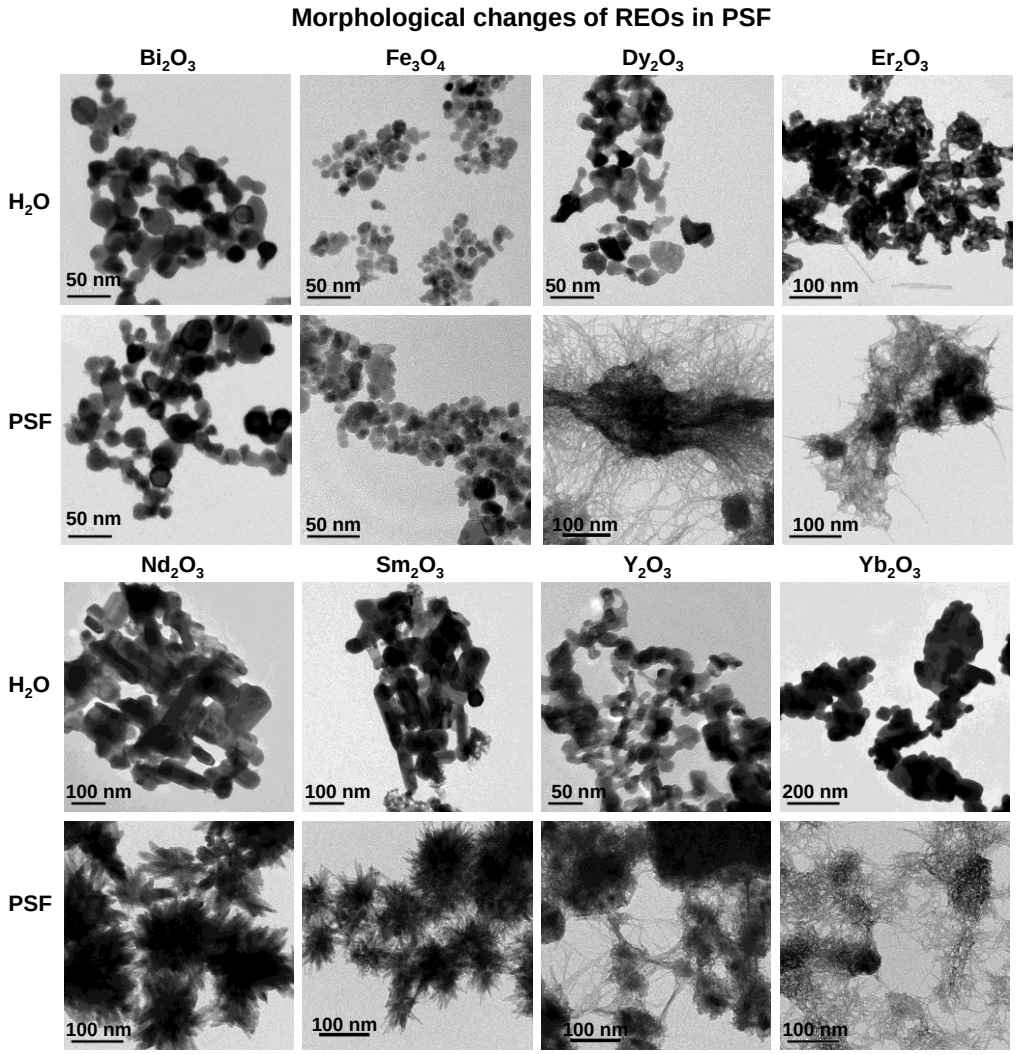

B

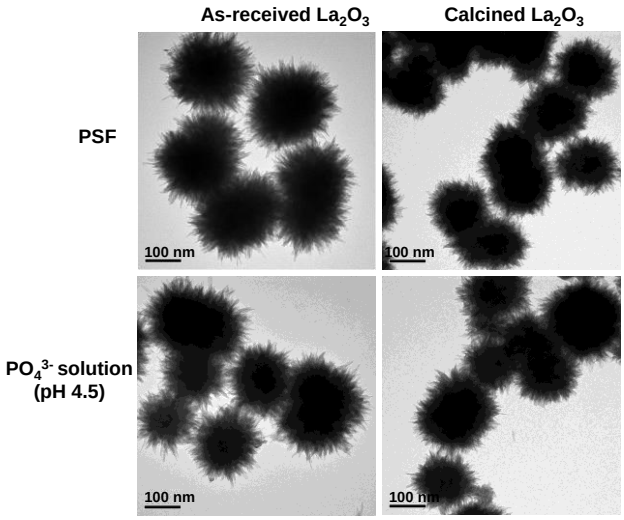

C

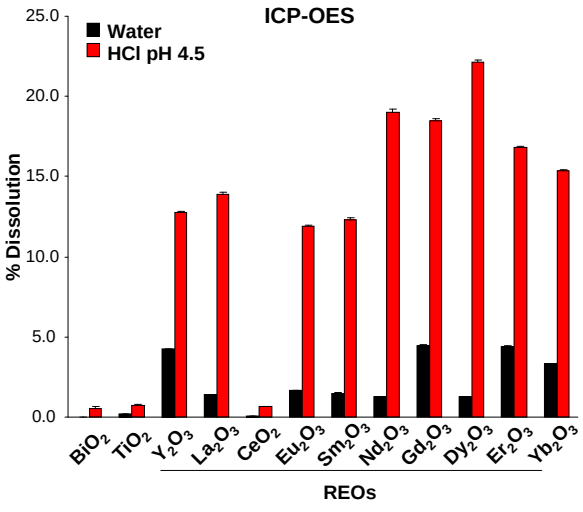

Figure S2

A

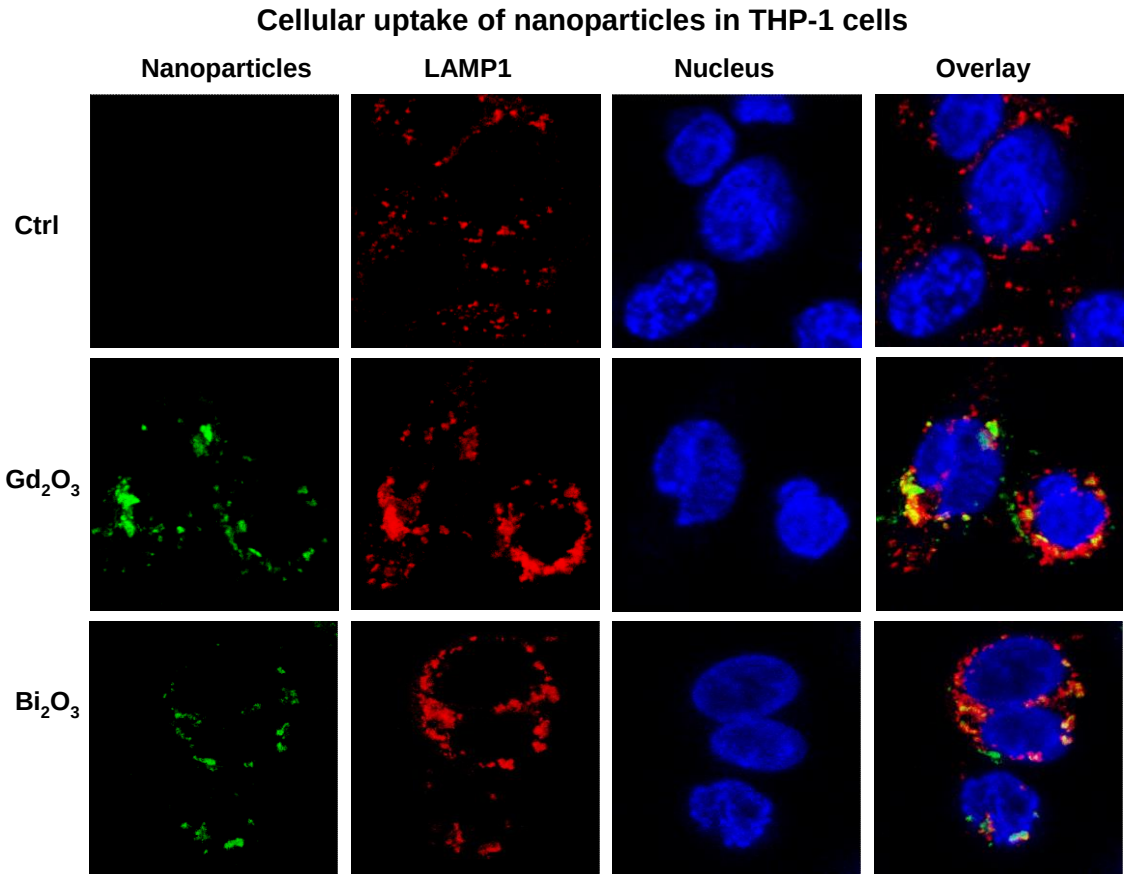
Cellular uptake of nanoparticles in THP-1 cells
Nanoparticles
LAMP1
Nucleus
Overlay
Ctrl
Gd_2O_3
Bi_2O_3

B

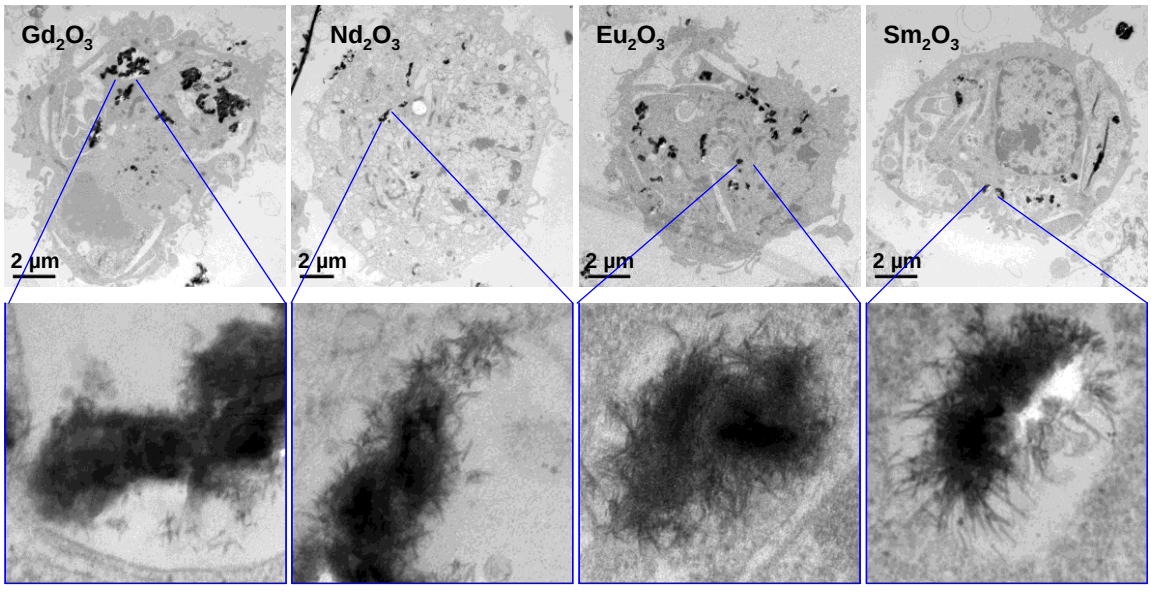
Bio-transformation of REOs in THP-1 cells
Gd_2O_3
Nd_2O_3
Eu_2O_3
Sm_2O_3
2 µm
2 µm
2 µm
2 µm

Figure S3

A

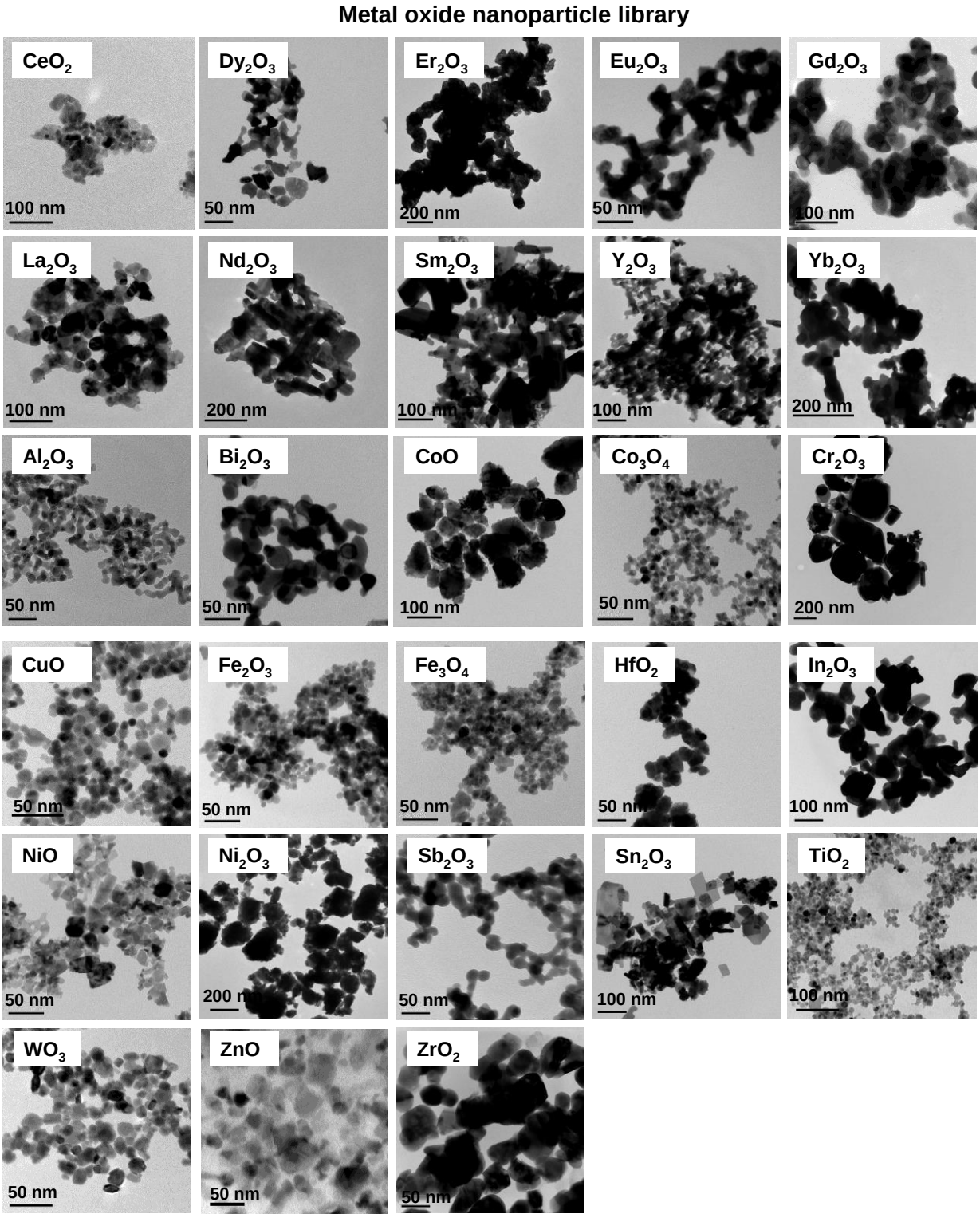
Metal oxide nanoparticle library
CeO2
100 nm
Dy2O3
50 nm
Er2O3
200 nm
Eu2O3
50 nm
Gd2O3
100 nm
La2O3
100 nm
Nd2O3
200 nm
Sm2O3
100 nm
Y2O3
100 nm
Yb2O3
200 nm
Al2O3
50 nm
Bi2O3
50 nm
CoO
100 nm
Co3O4
50 nm
Cr2O3
200 nm
CuO
50 nm
Fe2O3
50 nm
Fe3O4
50 nm
HfO2
50 nm
In2O3
100 nm
NiO
50 nm
Ni2O3
200 nm
Sb2O3
50 nm
Sn2O3
100 nm
TiO2
100 nm
WO3
50 nm
ZnO
50 nm
ZrO2
50 nm

B

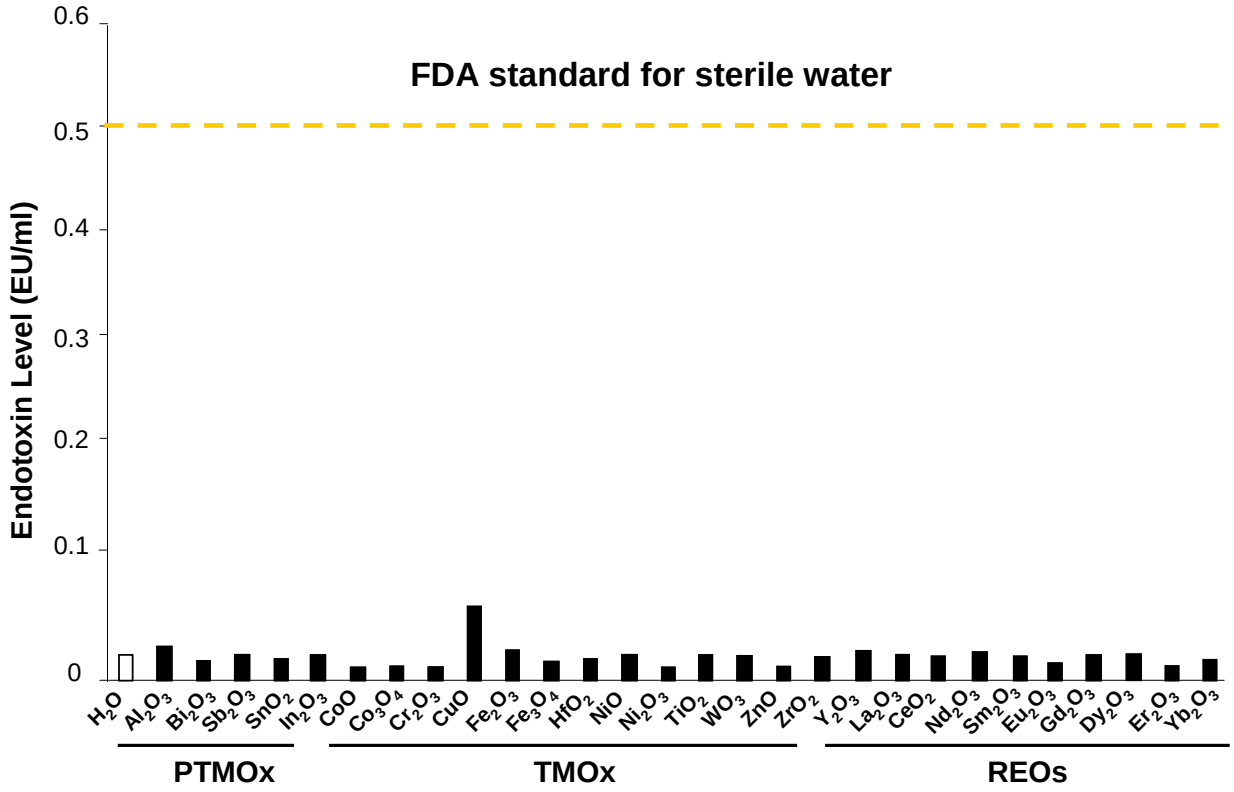
FDA standard for sterile water
Endotoxin Level (EU/ml)
0.6
0.5
0.4
0.3
0.2
0.1
0
H2O
Al2O3
Bi2O3
Sb2O3
SnO2
In2O3
CoO
Co3O4
Cr2O3
CuO
Fe2O3
Fe3O4
HfO2
NiO
Ni2O3
TiO2
WO3
ZnO
ZrO2
Y2O3
La2O3
CeO2
Nd2O3
Sm2O3
Eu2O3
Gd2O3
Dy2O3
Er2O3
Yb2O3
PTMOx
TMOx
REOs

C

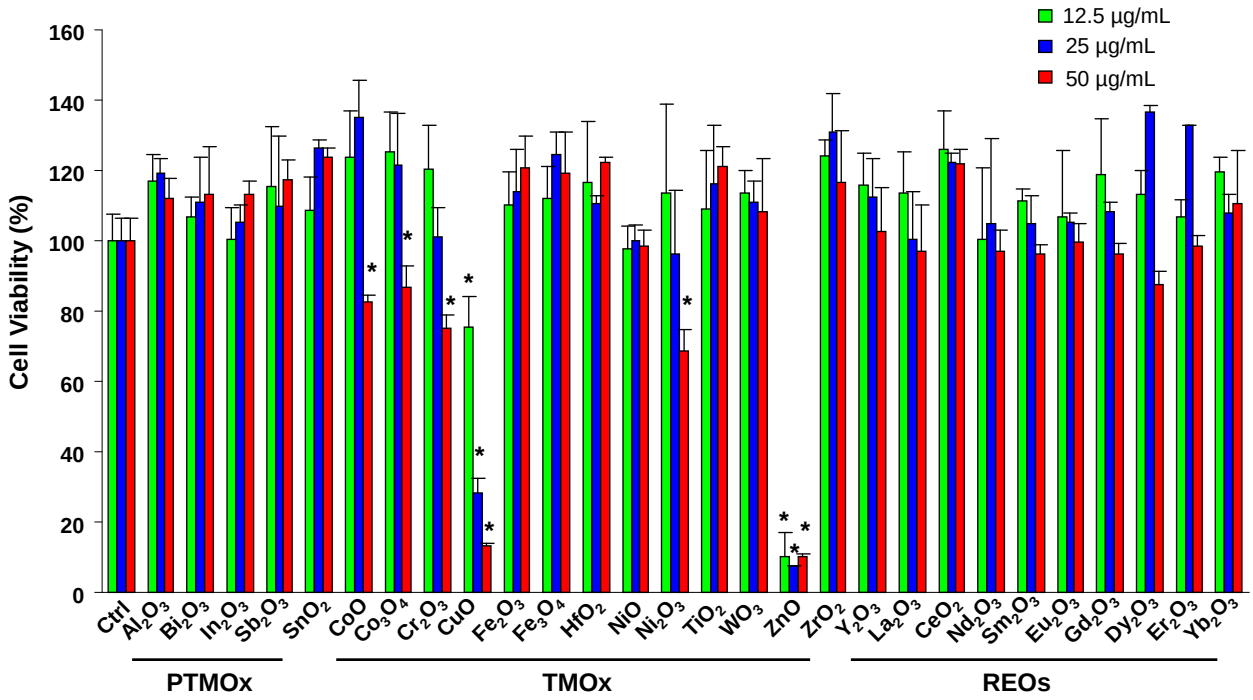
12.5 μg/mL
25 μg/mL
50 μg/mL
Cell Viability (%)
160
140
120
100
80
60
40
20
0
Ctrl
Al2O3
Bi2O3
In2O3
Sb2O3
SnO2
CoO
Co3O4
Cr2O3
CuO
Fe2O3
Fe3O4
HfO2
NiO
Ni2O3
TiO2
WO3
ZnO
ZrO2
Y2O3
La2O3
CeO2
Nd2O3
Sm2O3
Eu2O3
Gd2O3
Dy2O3
Er2O3
Yb2O3
PTMOx
TMOx
REOs

D

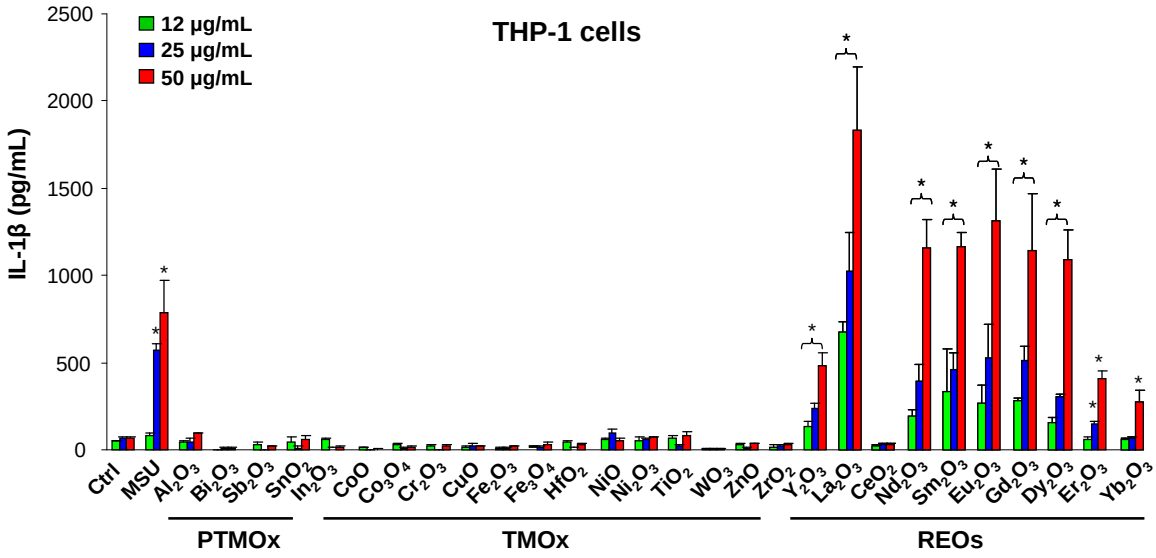
THP-1 cells
12 µg/mL
25 µg/mL
50 µg/mL
IL-1β (pg/mL)
2500
2000
1500
1000
500
0
Ctrl
MSU
Al2O3
Bi2O3
Sb2O3
SnO2
In2O3
CoO
Co3O4
Cr2O3
CuO
Fe2O3
Fe3O4
HfO2
NiO
Ni2O3
TiO2
WO3
ZnO
ZrO2
Y2O3
La2O3
CeO2
Nd2O3
Sm2O3
Eu2O3
Gd2O3
Dy2O3
Er2O3
Yb2O3
PTMOx
TMOx
REOs

E

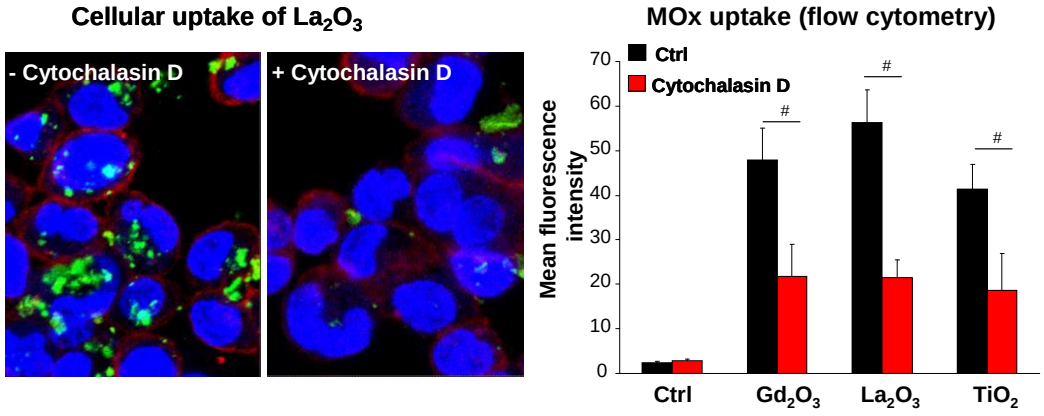
Cellular uptake of La2O3
- Cytochalasin D
+ Cytochalasin D
MOx uptake (flow cytometry)
Ctrl
Cytochalasin D
Mean fluorescence intensity
70
60
50
40
30
20
10
0
Ctrl
Gd2O3
La2O3
TiO2

F

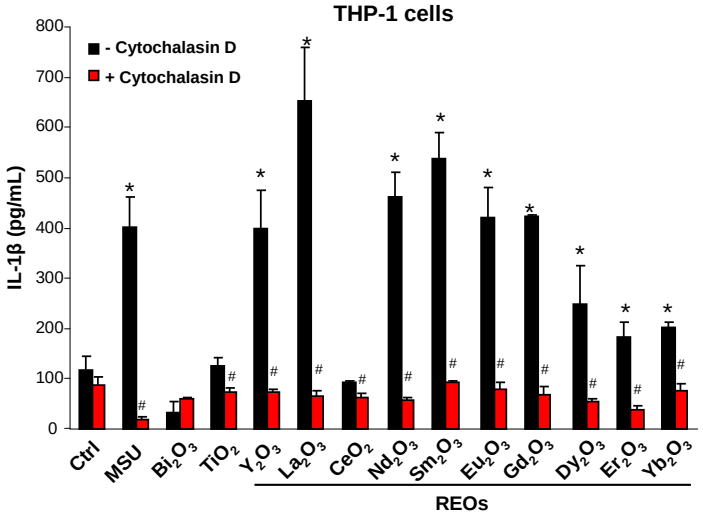
THP-1 cells
- Cytochalasin D
+ Cytochalasin D
IL-1β (pg/mL)
800
700
600
500
400
300
200
100
0
Ctrl
MSU
Bi2O3
TiO2
Y2O3
La2O3
CeO2
Nd2O3
Sm2O3
Eu2O3
Gd2O3
Dy2O3
Er2O3
Yb2O3
REOs

G

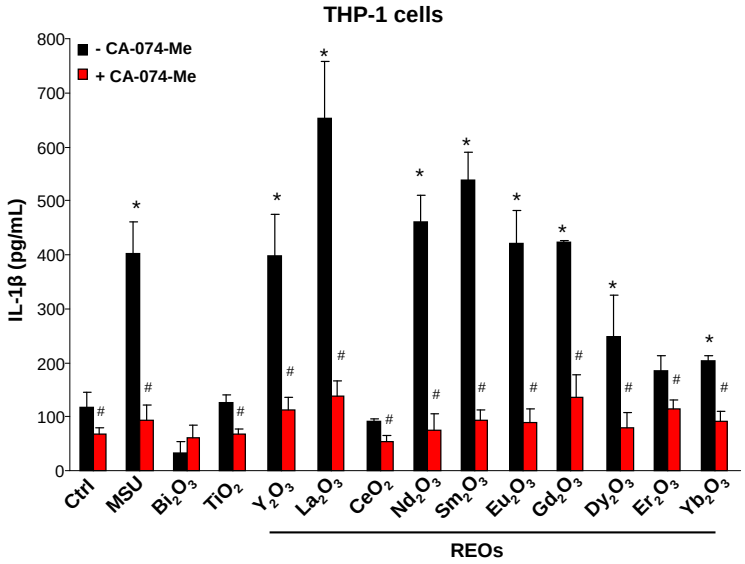
THP-1 cells
- CA-074-Me
+ CA-074-Me
IL-1β (pg/mL)
800
700
600
500
400
300
200
100
0
Ctrl
MSU
Bi2O3
TiO2
Y2O3
La2O3
CeO2
Nd2O3
Sm2O3
Eu2O3
Gd2O3
Dy2O3
Er2O3
Yb2O3
REOs

H

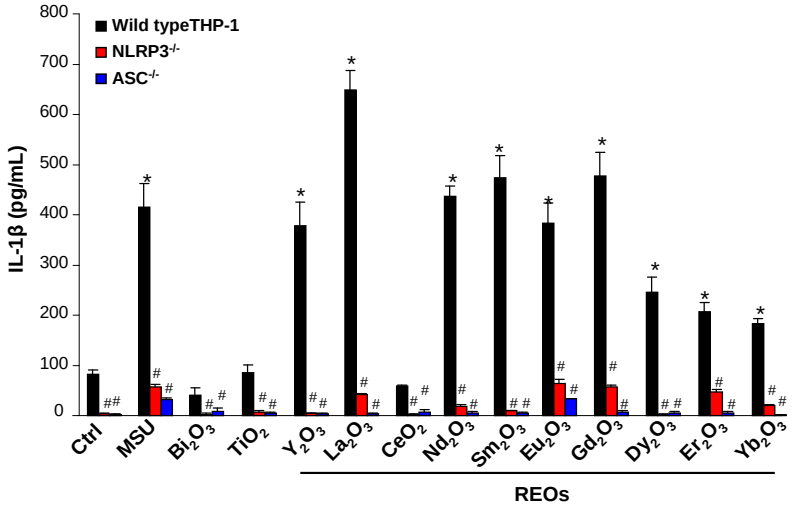
Wild typeTHP-1
NLRP3-/-
ASC-/-
IL-1β (pg/mL)
800
700
600
500
400
300
200
100
0
Ctrl
MSU
Bi2O3
TiO2
Y2O3
La2O3
CeO2
Nd2O3
Sm2O3
Eu2O3
Gd2O3
Dy2O3
Er2O3
Yb2O3
REOs

Figure S4

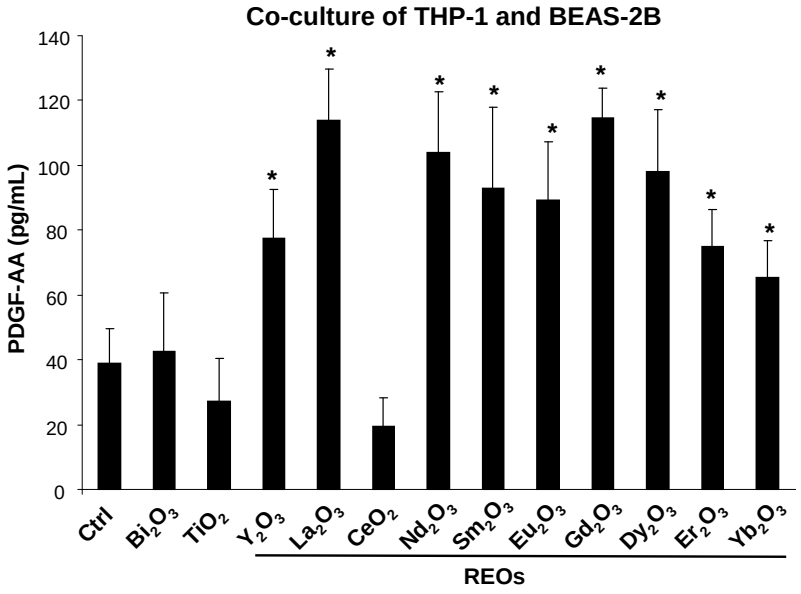
Co-culture of THP-1 and BEAS-2B
PDGF-AA (pg/mL)
140
120
100
80
60
40
20
0
Ctrl
Bi2O3
TiO2
Y2O3
La2O3
CeO2
Nd2O3
Sm2O3
Eu2O3
Gd2O3
Dy2O3
Er2O3
Yb2O3
REOs

Figure S5

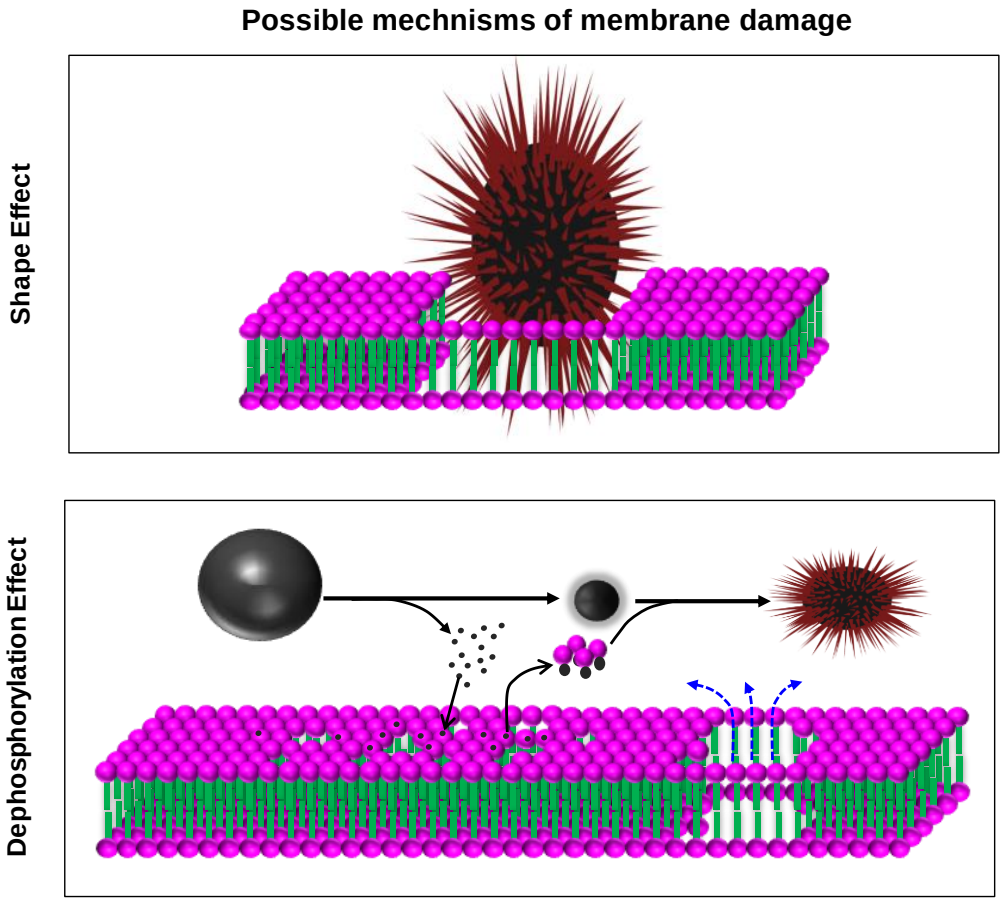
Possible mechnisms of membrane damage
Shape Effect
Dephosphorylation Effect

Figure S6

A

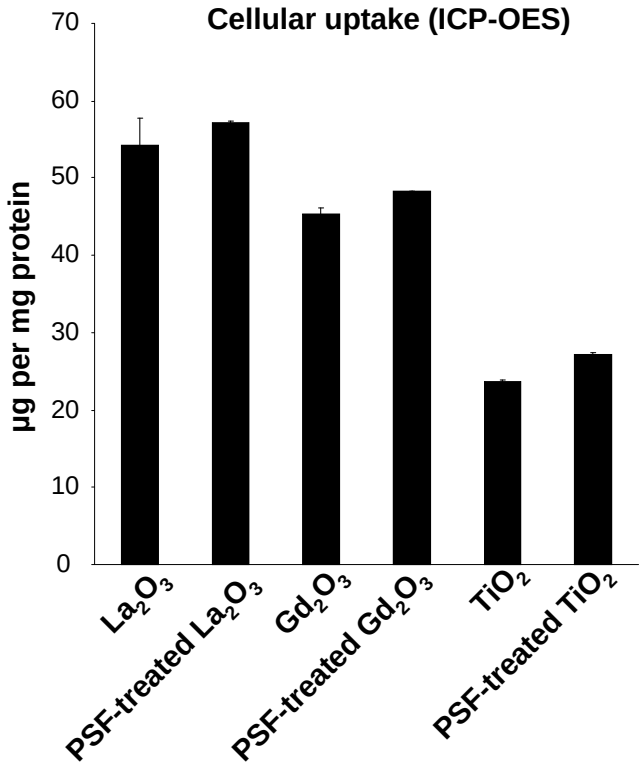
Cellular uptake (ICP-OES)
µg per mg protein
70
60
50
40
30
20
10
0
La2O3
PSF-treated La2O3
Gd2O3
PSF-treated Gd2O3
TiO2
PSF-treated TiO2

B

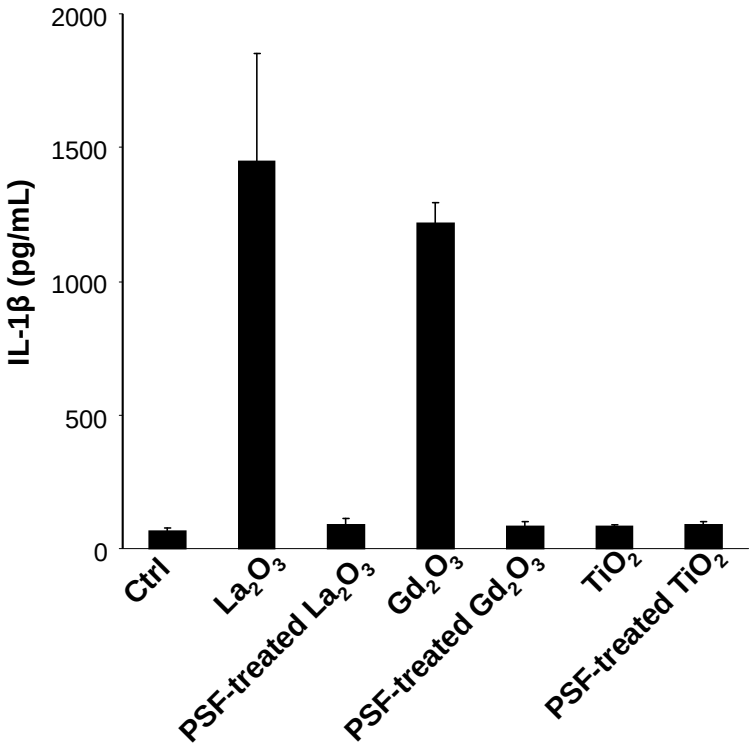
IL-1β (pg/mL)
2000
1500
1000
500
0
Ctrl
La2O3
PSF-treated La2O3
Gd2O3
PSF-treated Gd2O3
TiO2
PSF-treated TiO2

Figure S7

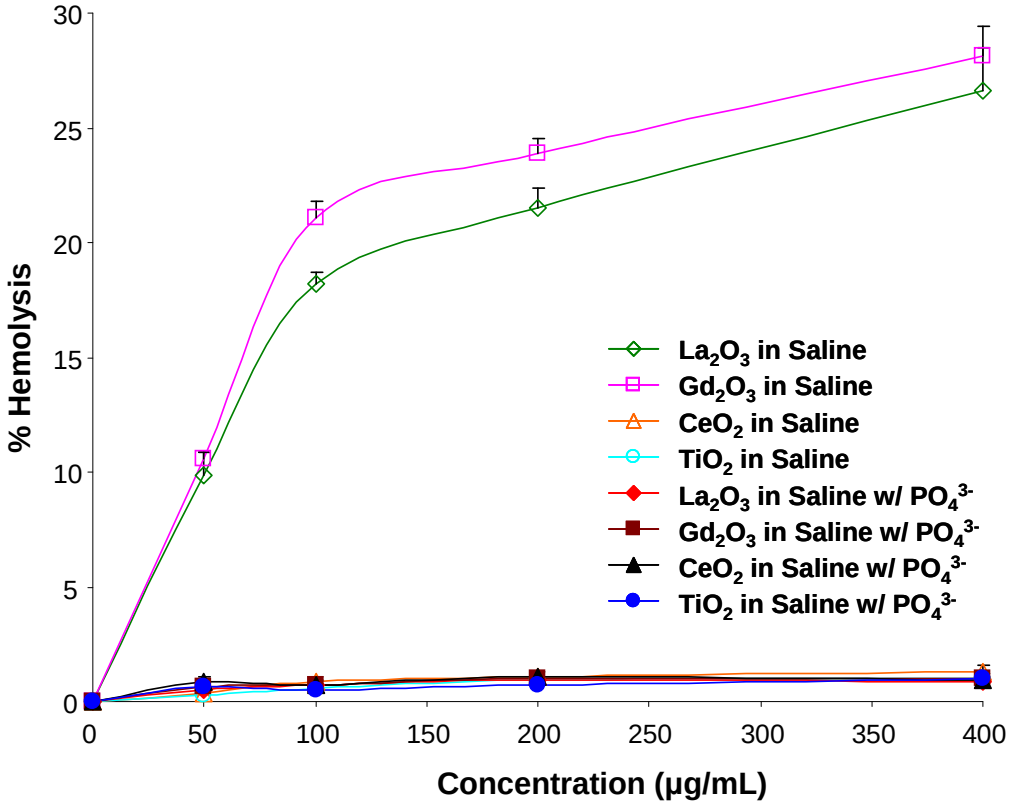
30
25
20
15
10
5
0
% Hemolysis
0
50
100
150
200
250
300
350
400
Concentration (µg/mL)
La2O3 in Saline
Gd2O3 in Saline
CeO2 in Saline
TiO2 in Saline
La2O3 in Saline w/ PO4 3-
Gd2O3 in Saline w/ PO4 3-
CeO2 in Saline w/ PO4 3-
TiO2 in Saline w/ PO4 3-

Figure S8

A

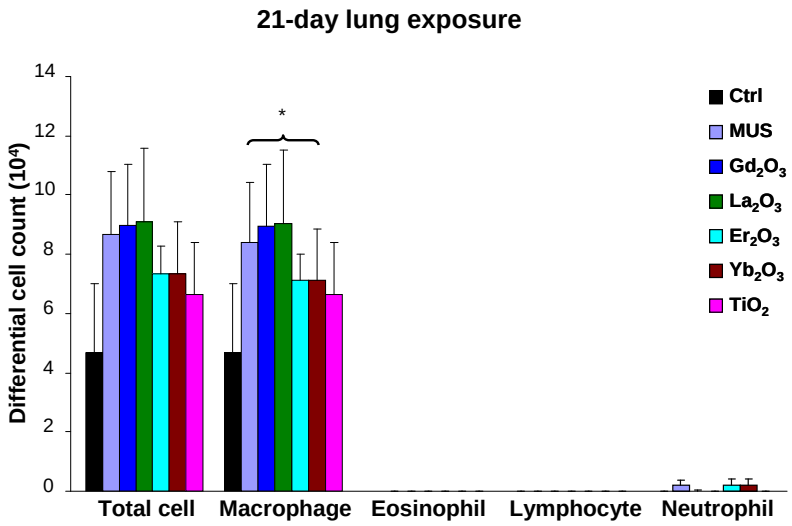
21-day lung exposure
Differential cell count (10⁴)
14
12
10
8
6
4
2
0
*
Ctrl
MUS
Gd2O3
La2O3
Er2O3
Yb2O3
TiO2
Total cell
Macrophage
Eosinophil
Lymphocyte
Neutrophil

B

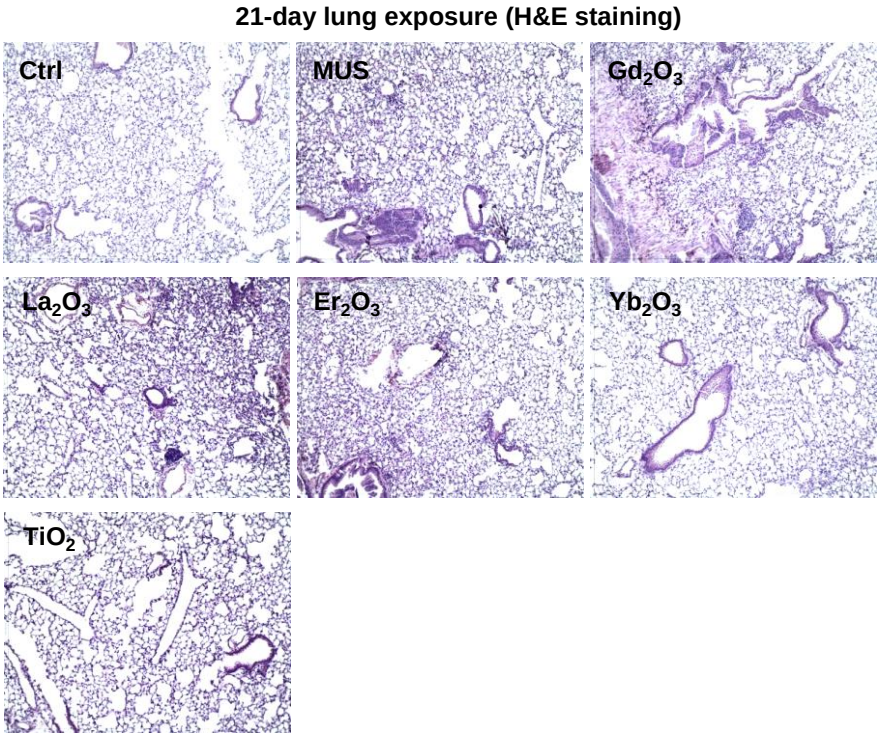
21-day lung exposure (H&E staining)
Ctrl
MUS
Gd2O3
La2O3
Er2O3
Yb2O3
TiO2

Figure S9

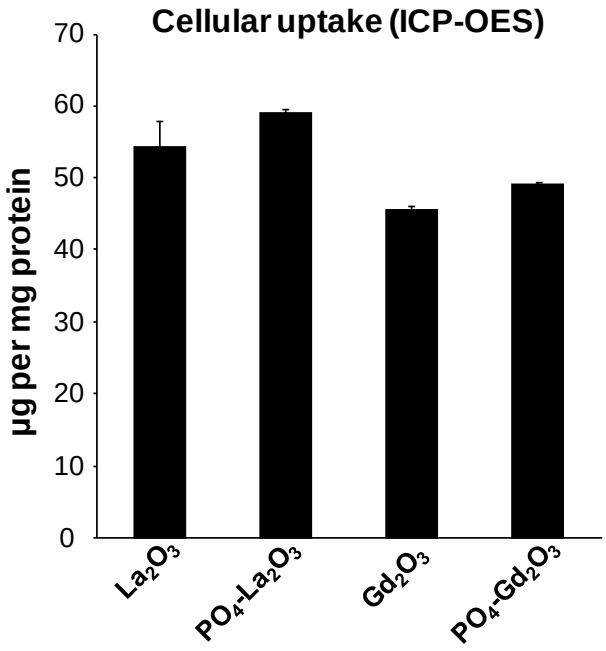
Cellular uptake (ICP-OES)
µg per mg protein
70
60
50
40
30
20
10
0
La2O3
PO4-La2O3
Gd2O3
PO4-Gd2O3

Figure S10

A

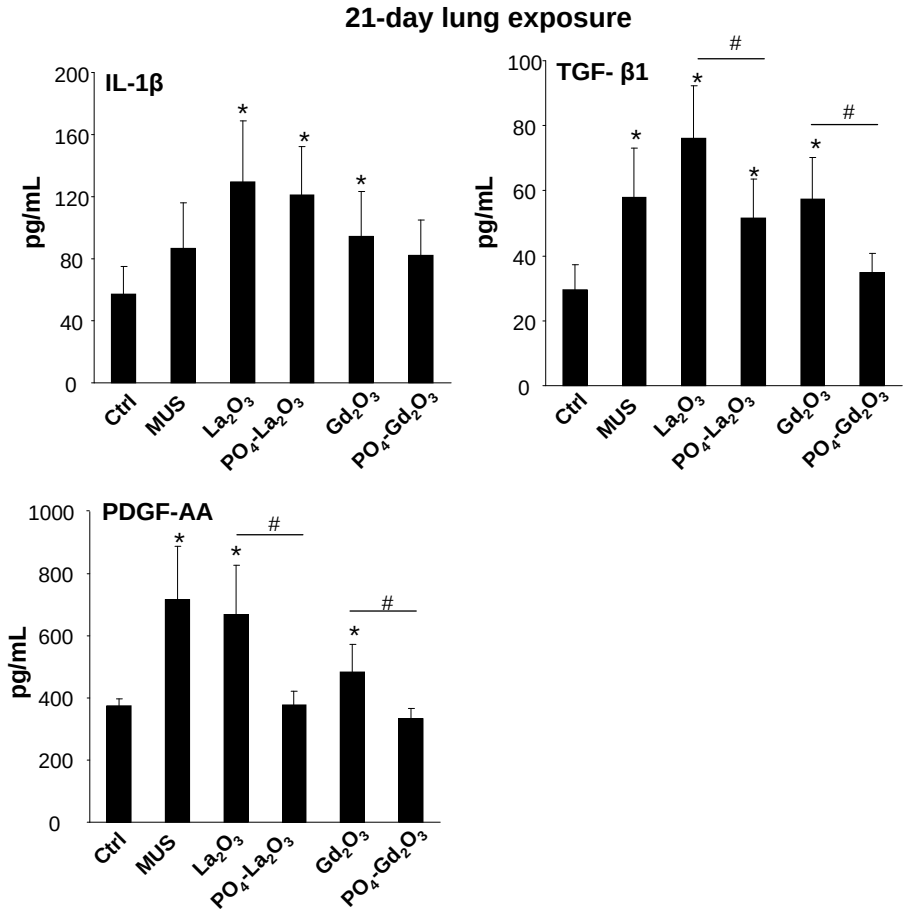

B

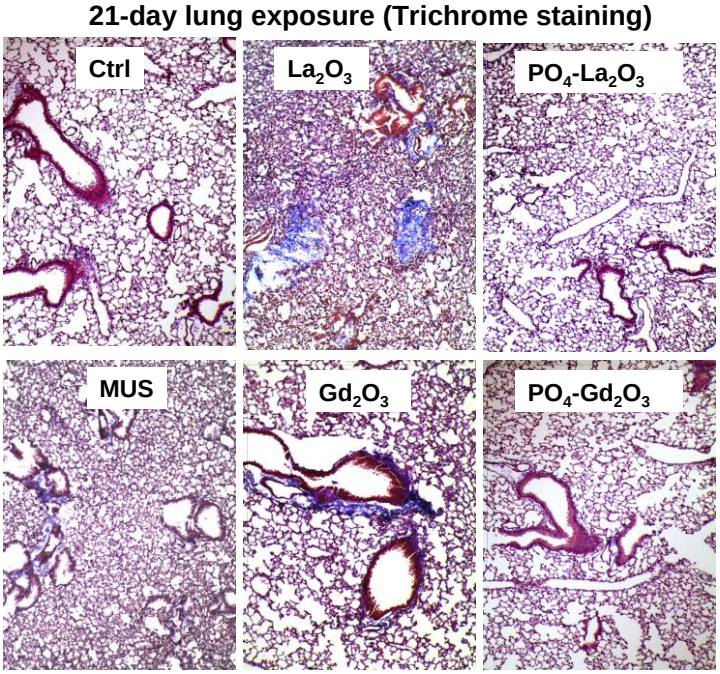

References

1. Wong, J. P.; Yang, H. M.; Blasetti, K. L.; Schnell, G.; Conley, J.Schofield, L. N. Liposome Delivery of Ciprofloxacin against Intracellular Francisella Tularensis Infection. *J. Control. Release* **2003,** *92*, 265-273.
2. Li, R.; Wang, X.; Ji, Z.; Sun, B.; Zhang, H.; Chang, C. H.; Lin, S.; Meng, H.; Liao, Y. P.; Wang, M.; *et al.* Surface Charge and Cellular Processing of Covalently Functionalized Multiwall Carbon Nanotubes Determine Pulmonary Toxicity. *Acs Nano* **2013,** *7*, 2352-2368.
3. Wang, X.; Xia, T.; Duch, M. C.; Ji, Z. X.; Zhang, H. Y.; Li, R. B.; Sun, B. B.; Lin, S. J.; Meng, H.; Liao, Y. P.; *et al.* Pluronic F108 Coating Decreases the Lung Fibrosis Potential of Multiwall Carbon Nanotubes by Reducing Lysosomal Injury. *Nano Lett.* **2012,** *12*, 3050-3061.
4. Wang, X.; Ji, Z.; Chang, C. H.; Zhang, H.; Wang, M.; Liao, Y. P.; Lin, S.; Meng, H.; Li, R.; Sun, B.; *et al.* Use of Coated Silver Nanoparticles to Understand the Relationship of Particle Dissolution and Bioavailability to Cell and Lung Toxicological Potential. *Small* **2013**.